Int. J. Electrochem. Sci., 16 **(2021)** Article ID: 210254, doi: 10.20964/2021.02.57

International Journal of
ELECTROCHEMICAL
SCIENCE
www.electrochemsci.org

Controllable Synthesis of Nickel Sulfide Nanosheet/Carbon Fibers Composite and Its Electrochemical Performances

Yuxuan Zhu, Dong Xiang[*], *Shaoqun Ma, Yue Wang, Hongzhi Li, Zhan Jiang*

School of Material Science and Engineering, Shandong Jianzhu University, Jinan 250101, People's Republic of China
[*]E-mail: xiang@sdjzu.edu.cn

Received: 7 November 2020 / *Accepted:* 23 December 2020 / *Published:* 31 December 2020

Nickel sulfide (NiS) nanosheet on carbon fibers (CFs) was prepared by using the hydrothermal method. By varying the concentration ratios, the morphology and size of NiS could be effectively controlled, which was conducive to the improvement of the electrochemical performance. The experimental findings revealed the formation of the uniformly distributed NiS nanosheet on the surface of the pre-treated carbon fibers, and the average NiS size for 2-NiS/CFs was about 200 nm. The specific capacitance of 2-NiS/CFs could reach 534.8 $F \cdot g^{-1}$ at 1 $A \cdot g^{-1}$. Further, the composite material could maintain its capacitance retention rate of 86% after 2000 cycles. Moreover, the supercapacitor exhibited a high energy density of 18.7 $Wh \cdot kg^{-1}$ at a power density of 252 $W \cdot kg^{-1}$. The unique structure of the NiS nanosheet/CFs electrode materials accelerated the electrochemical reaction between the electrolyte and electrode. The pseudo-capacitance of the composite materials is needed to be improved further.

Keywords: supercapacitor, carbon fiber, nickel sulfide, nanosheet, electrochemical

1. INTRODUCTION

Supercapacitors, also known as electrochemical capacitors, exhibit advantages of short charging duration, wide operating temperature range, high power density and long storage life. As a result, these materials have attracted a significant attention in many industries, including electric power, communication services, automobile industry, etc. [1-3]. However, overcoming the challenges of low energy density, poor flexible and wearability as well as applying these materials in real life are still needed to be accomplished.

In general, the electrode materials, such as carbon, conductive polymers and metal compounds, are the core components of supercapacitors, [4-6]. The carbon materials have high conductivity, a wide range of raw material sources, low preparation cost and environmentally friendliness [7-10]. Hence, these materials have been extensively used to develop the electrode materials for supercapacitors[11-13]. However, the low specific capacitance and energy density hinder their widespread practical

applications[14-17]. Further, the metal sulfides exhibit higher capacitance and electrochemical activity than the carbon materials, along with superior conductivity and lower electronegativity than the other metal compounds, thus, making these materials the object of intense researches [18-20]. The common metal sulfides include nickel sulfide (NiS), cobalt sulfide (CoS) and molybdenum sulfide (MoS). Among these, NiS plays an importance role in the development of the electrode materials due to its high conductivity, low cost and low toxicity[21-23]. It is considered to be a promising pseudo-capacitance material and can be used to improve the specific capacitance of supercapacitors[24-27]. However, the low cycle stability during operation is currently the main barrier for the development of pure NiS as an effective electrode material[28-30]. To overcome this challenge, the carbon materials have been employed as a conductive substrate and to form composite with NiS. Wu et al.[31] used a facile low-temperature water-bath method to synthesize the interconnected NiS@C. The hybrid structure displayed a high specific capacitance of 1827 $F \cdot g^{-1}$ at 1 $A \cdot g^{-1}$. In addition, it exhibited an excellent cyclic stability of 72% at 20 $A \cdot g^{-1}$ after 5000 cycles. In order to achieve the flexibility and wearability in supercapacitors, the composite of carbon fibers and metal sulfides has been explored. Using pure carbon fibers as a soft supercapacitor electrode, the contribution of the electric double layer to the capacity is generally limited. In most cases, the carbon fibers are used as a carrier for supporting the other active materials[12,32]. The metal sulfides are needed to be deposited on the carbon fiber materials to enhance the capacitance and achieve an excellent electrochemical performance[9,33]. Dhaiveegan et al. [34] used a simple one-step method to deposit the nanoporous mesh Ni_3S_2 films on the flexible carbon fiber cloth (CFC). For the current density of the Ni_3S_2 electrode of 1 $A \cdot g^{-1}$, an excellent specific capacitance of about 600 $F \cdot g^{-1}$ was achieved. In addition, the capacitance retention rate was still 84.6% after testing the Ni_3S_2 electrode for 2000 cycles at a current of 2 $A \cdot g^{-1}$. Upadhyay et al. [35] prepared the MoS_2 nanosheet electrode material on the carbon fiber paper (CFP) by using the hydrothermal method. For the current density of 2 $A \cdot g^{-1}$, the specific capacitance was determined to be 249 $F \cdot g^{-1}$. In addition, the initial capacitance remained only 41.3% at the current density of 10 $A \cdot g^{-1}$.

In this paper, the hydrothermal method was used to prepare the NiS/CFs nanosheet composites with controllable behavior. The electrochemical performance of the NiS/CFs composites was tested by using electrochemical impedance spectroscopy (EIS), cyclic voltammetry (CVs) and galvanostatic charge/discharge methods. 2-NiS/CFs was observed to possess a large electrochemical capacitance in the alkaline electrolyte (3 $mol \cdot L^{-1}$ KOH). For the current density of 1 $A \cdot g^{-1}$, the specific capacitance of 2-NiS/CFs was 534.8 $F \cdot g^{-1}$. At the same time, the electrode exhibited an excellent electrochemical performance.

2. EXPERIMENTAL

2.1. Preparation of NiS/CFs electrode

2.1.1. Pretreatment of CFs

CFs used in the study had a diameter of about 10 μm. The fiber surface was smooth and contained several oxide films. As a result, it was difficult to bond the active substances to CFs. The

fibers were immersed in a 3 mol·L^{-1} acetone solution at different temperatures. After several trials, 60 °C was determined to be the optimal temperature, with the suitable holding time is 6 h. The surface of CFs was coarsened by electrochemical anodic oxidation in a 3 mol·L^{-1} potassium hydroxide solution. The optimal coarsening voltage and duration were 2.5 V and 5 min, respectively.

2.1.2. Preparation of NiS/CFs composite materials

The composite electrode materials were prepared by using a two-step hydrothermal method, as shown in Figure 1. In the first step, $Ni(CH_3COO)_2$ and NH_4F in the molar ratio of 1:4 were added to the deionized water. Subsequently, the mixed solution was transferred to a 25 mL autoclave and was placed in a thermostat. The holding temperature and time were 180 °C and 5 h, respectively. $Ni(OH)_2$ could be obtained as per equations (1) and (2).

$$CH_3COO^- + H_2O + F^- + NH_4^+ \rightarrow HF + CH_3COOH + OH^- + NH_3\uparrow \quad (1)$$

$$Ni^{2+} + 2OH^- \rightarrow Ni(OH)_2\downarrow \quad (2)$$

In the second step, the prepared $Ni(OH)_2$ was added to the $Na_2S{\cdot}9H_2O$ solutions with different molar concentrations (1, 2, and 3 mol·L^{-1}).

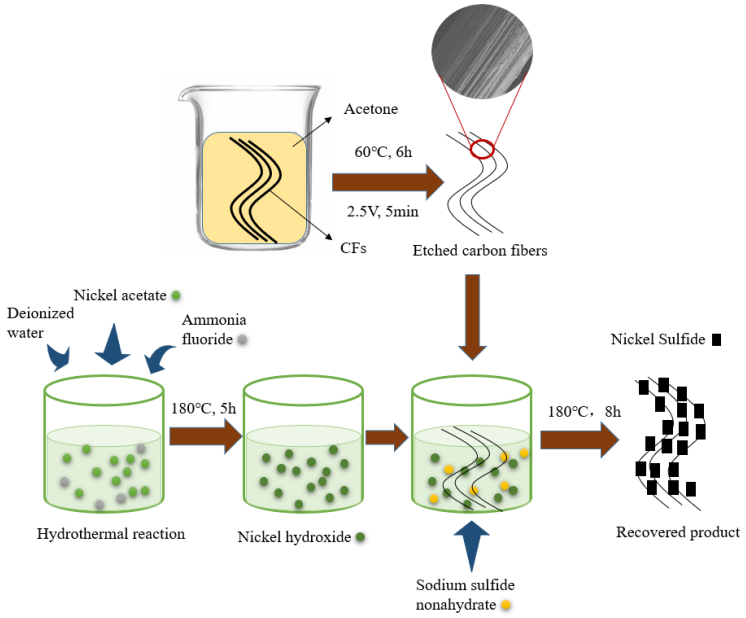

Figure 1. The schematic of the synthesis of the NiS/CFs electrode materials

The as-obtained mixed solutions and coarsened CFs were transferred to a 25 mL autoclave, stored in a drying oven at 180 °C for 8 h, followed by cooling to room temperature. The NiS/CFs composite materials were obtained as per equation (3). The products were named 1-NiS/CFs, 2-NiS/CFs, and 3-NiS/CFs.

$$Ni(OH)_2 + S^{2-} + 2Na^+ \rightarrow NiS\downarrow + 2Na^+ + 2OH^- \quad (3)$$

The specific capacitance (C, $F \cdot g^{-1}$) of the supercapacitor could be calculated by using the relevant relation [36].

The energy density (E, $Wh \cdot kg^{-1}$) and corresponding power density (P, $W \cdot kg^{-1}$) were calculated by using the following relations [36].

$$E = \frac{C \times \Delta V^2}{2} \quad (4)$$

$$P = \frac{E}{\Delta t} \quad (5)$$

where ΔV is the potential difference and Δt(s) is the discharge duration during the charging and discharging processes.

2.2. Physical properties of materials

The structure, phase composition and morphology of the samples were characterized by X-ray diffraction (XRD, Rigaku D/max-2500, Cu $K\alpha$ ray) and field emission scanning electron microscope (FE-SEM, SU-8010). The elemental composition of the electrode materials was analyzed by X-ray energy spectrometer (EDS, SU-70).

2.3. Analysis of electrochemical performances

The samples were analyzed by using a three-electrode electrochemical workstation (CHI660E). In the three-electrode system, a saturated calomel electrode worked as the reference electrode, a Pt sheet was used as the auxiliary electrode, and the electrolyte was a 3 $mol \cdot L^{-1}$ KOH solution. Under the open-circuit voltage, the electrochemical workstation was used to carry out the electrochemical impedance spectroscopy (EIS) analysis of the samples with an excitation signal from 10 kHz to 100 MHz in a 3 mol L^{-1} KOH solution. Zsimpwin 3.0 software (Echem Software) was used to transform the impedance data into the equivalent circuit. The cyclic voltammetry (CV) curves were recorded by using the electrochemical workstation in the voltage range -0.8~0.2 V at different scan rates. The galvanostatic charge-discharge capacitance (C_s) was also measured by using the electrochemical workstation. The charging and discharging voltage range was from -0.8 to 0.2 V.

3. RESULTS AND DISCUSSION

3.1. Structural characterization

Figure 2 shows X-ray diffraction (XRD) patterns of the NiS/CFs composites (1-NiS/CFs, 2-NiS/CFs and 3-NiS/CFs). The 2θ peaks at 18.44°, 40.45° and 72.62° are observed in the samples, with the corresponding crystal faces (110), (211) and (312), respectively. The peak values are noted to agree well with the peaks of NiS in the 12-0041 standard card of PDF. It indicates that $Ni(OH)_2$, formed by

the chemical reaction, is completely converted to NiS and subsequently combines with CFs to form the NiS/CFs electrode materials.

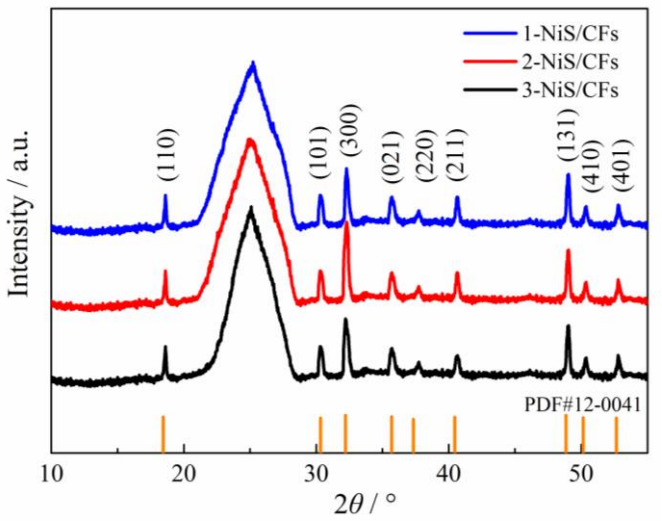

Figure 2. X-ray diffraction (XRD) patterns of the NiS/CFs composites

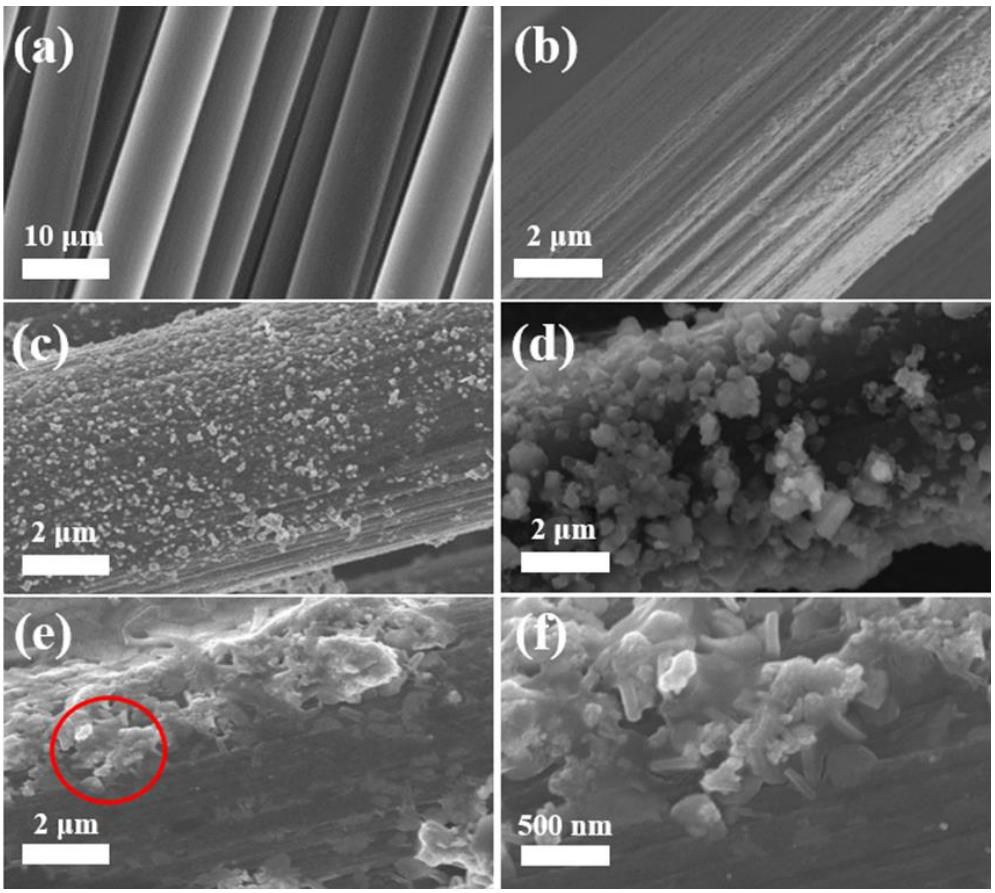

Figure 3. Scanning electron micrographs (SEM) of the unprocessed CFs (**a**), CFs after coarsening (**b**), 1-NiS/CFs (**c**), 3-NiS/CFs (**d**) and 2-NiS/CFs **(e)-(f)**.

The scanning electron micrographs of the carbon fibers and their composites are demonstrated in Figure 3. It can be observed from Figure 3(a) that the untreated carbon fibers possess a smooth surface and uniform thickness, with a diameter of~10 μm. The morphology of the coarsened carbon fibers is presented in Figure 3(b), and numerous deep gullies can be clearly observed. Figure 3(c) shows the small sized NiS particles on CFs for the 1-NiS/CFs composites, due to the low content of S in the solution not sufficient to cover the entire surface of carbon fibers. Furthermore, as the S concentration is too high, the active material in 3-NiS/CFs is noted to be aggregated into large particles, with non-uniform distribution and unsatisfactory inter-particle combinations. A dense film is noted to be formed on the surface of CFs in 2-NiS/CFs, with the film composed of NiS nanosheets, as shown in Figures 3(e) and (f). The average size of NiS nanosheets is determined to be 200 nm. The observed morphology facilitates the transmission and storage of electrons. Hence, the composition ratio in 2-NiS/CFs is concluded to be conductive for achieving an enhanced performance.

As shown in Figure 4, the element distribution of 2-NiS/CFs electrode material was analyzed by energy dispersive spectrometry (EDS). Figure 4(a) presents the EDS spectrum of 2-NiS/CFs, whereas Figures 4(b)-(d) exhibit the EDS elemental mapping images for C, S and Ni. As can be observed, the S and Ni elements are confirmed to be present on the surface of CFs.

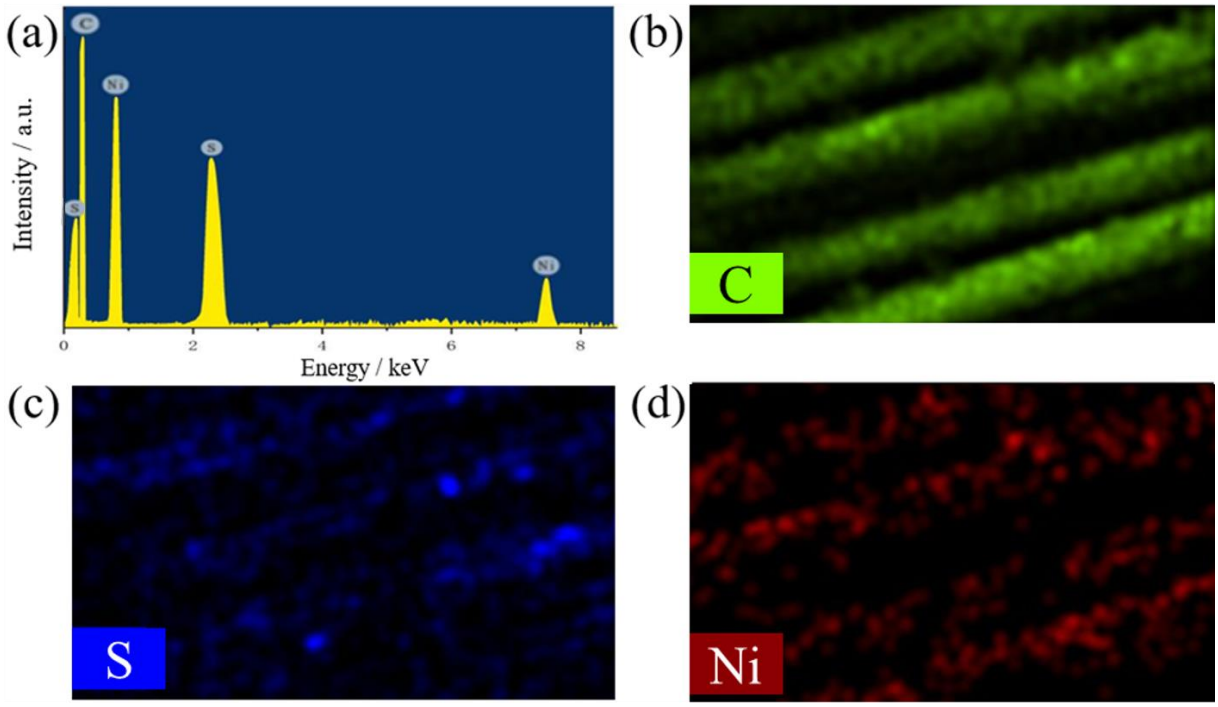

Figure 4. EDS spectrum of 2-NiS/CFs (**a**) and elemental mapping images of 2-NiS/CFs for C (**b),** S **(c)** and Ni **(d**).

3.2. Electrochemical analysis

Figure 5 shows the AC impedance curves (EIS) of the 1-NiS/CFs, 2-NiS/CFs and 3-NiS/CFs samples. As can be observed, all samples exhibited similar impedance shapes. Generally, the

impedance of the Nyquist plot is semicircular in the high-frequency region. The semicircle is driven by the charge transfer process, which is expressed as the EIS spectrum (R_{ct}). The approximately 45° straight line represents the diffusion process similar to the spherical diffusion, namely, the Warburg impedance (W)[37]. The equivalent fitting circuit is present in the inset of Figure 5. By calculation, the R_{ct} values of 1-NiS/CFs, 2-NiS/CFs and 3-NiS/CFs are determined to be 3.87, 1.26 and 2.48 Ω cm^2, respectively. It can be observed that 2-NiS/CFs electrode material exhibits the smallest impedance value, which promotes the charge transfer and leads to a high conductivity.

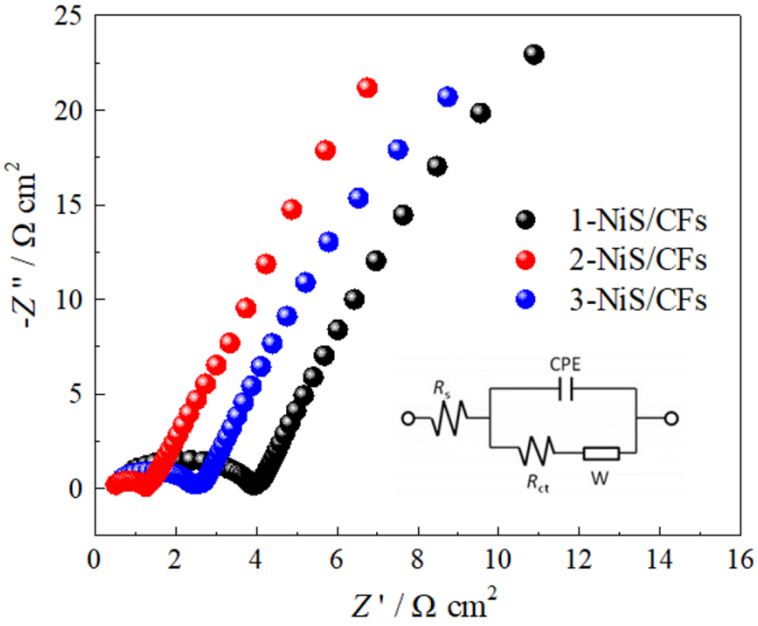

Figure 5. Nyquist plot of the NiS/CFs electrodes tested in a 3 mol·L^{-1} KOH solution. The equivalent circuit of the fitted impedance spectra is also presented.

Figure 6 shows the CV curves of 1-NiS/CFs, 2-NiS/CFs and 3-NiS/CFs electrodes at different scanning speeds. As shown in Figure 6(a), 1-NiS/CFs possesses a low extent of surface-active substance and redox process, which shows the characteristics of the electric double layer. In Figures 6(b) and (c), under guaranteeing the condition of a particular rectangular shape, in the voltage range -0.6-0.0 V, the CV curves of the 2-NiS/CFs and 3-NiS/CFs composites exhibit the redox peaks. This indicates that the 2-NiS/CFs and 3-NiS/CFs electrodes possess the properties of the capacitor electric double layer and pseudo-capacitance of the metal sulfide. In addition, the formed NiS nanosheet is noted to be uniformly distributed on the surface of the carbon fibers, thus, providing numerous energy storage locations. The composite material can lead to a high current intensity within a specific voltage range. It can be observed from Figure 6(d) that when a scanning speed of the composite electrodes is at 10 mV·s^{-1}, the specific capacitance of 2-NiS/CFs is higher than that of 1-NiS/CFs and 3-NiS/CFs composite electrodes. These results indicate that the uniformly distributed NiS nanosheet can enhance the capacitance and improve the energy storage performance in the 2-NiS/CFs composite material.

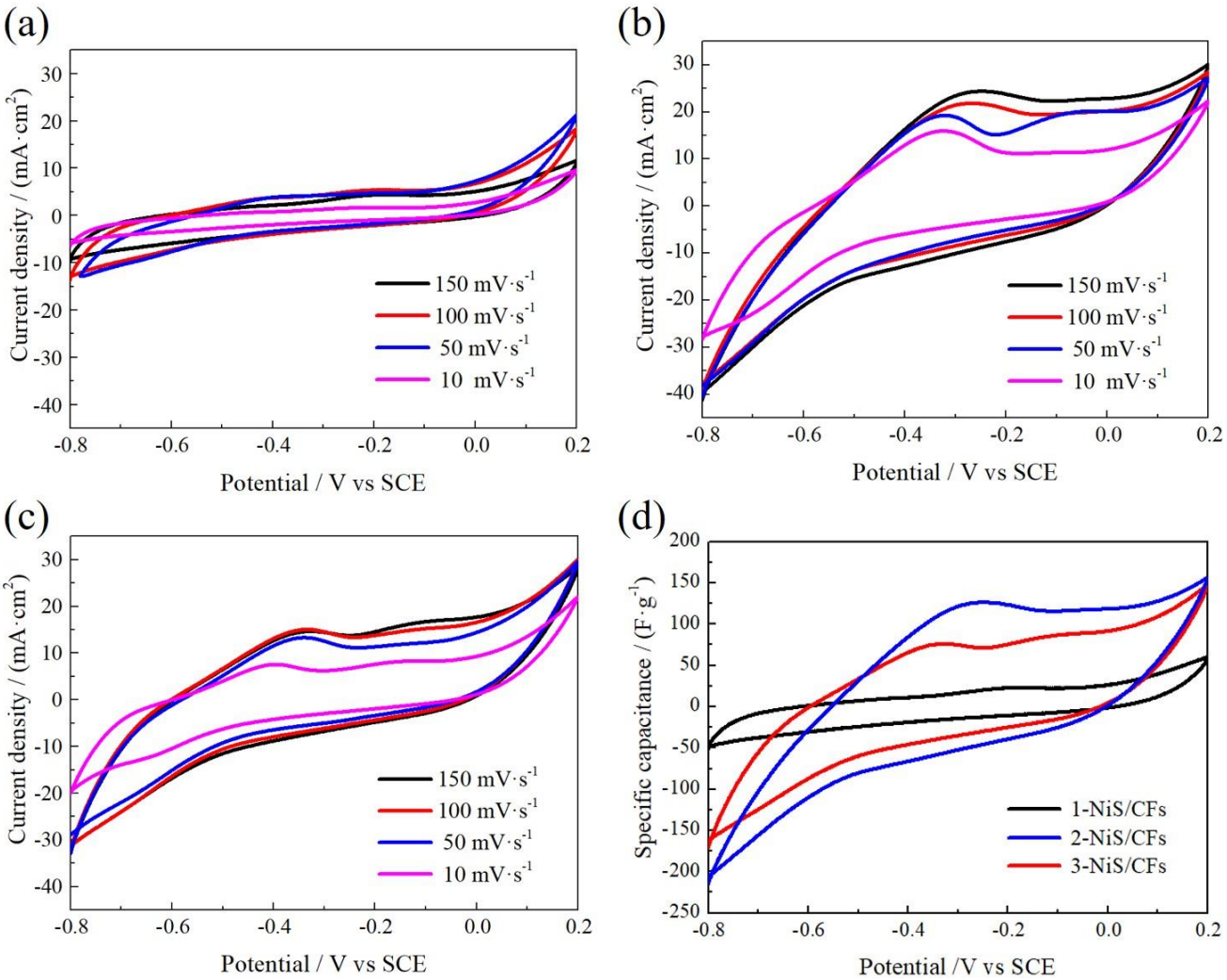

Figure 6. CV curves of 1-NiS/CFs (**a)**, 2-NiS/CFs (**b)** and 3-NiS/CFs (**c)** at different scanning speeds (10, 50, 100 and 150 mV·s^{-1}) in a 3 mol·L^{-1} of KOH solution, and the specific capacitance of 1-NiS/CFs, 2-NiS/CFs and 3-NiS/CFs at a scanning speed of 10 mV·s^{-1} (**d)**.

Figure 7 shows the galvanostatic charge and discharge behavior, specific capacitance and cyclic performance of 1-NiS/CFs, 2-NiS/CFs and 3-NiS/CFs in a 3 mol·L^{-1} KOH solution at different current densities. Figure 7 (a-c) demonstrate the charging and discharging duration of the composite electrode materials as a function of the current density. On increasing the current density, the charging and discharging duration of the composite electrode materials is observed to continuously decrease. Further, Figure 7(d) reveals that 2-NiS/CFs exhibits the longest charge-discharge duration at a current density of 1 A·g^{-1}, reaching 330.9 s. The maximum specific capacitance of 2-NiS/CFs is noted to 534.8 F·g^{-1}, which is 1.4 and 2.6 times higher than the values observed for 3-NiS/CFs and 1-NiS/CFs (383.3 and 203 F·g^{-1}), respectively. Figure 7(e) shows the specific capacitance of the composite materials at different current densities. The 2-NiS/CFs composite is noted to exhibit the superior specific capacitance at the same current density as compared to other materials. In order to determine the cycle stability of the electrode materials, the 2-NiS/CFs composite was charged and discharged in a 3 mol·L^{-1} KOH solution for multiple cycles. The first ten charge-discharge cycles are presented in Figure 7(f). As the number of charge-discharge cycles increases, the limited capacity of the 2-NiS/CFs electrode is

noted to gradually decrease. After 2000 cycles, the capacitance value is observed to be 86% of the initial value, which represents a beneficial behavior as compared with the previous literature reports [34].

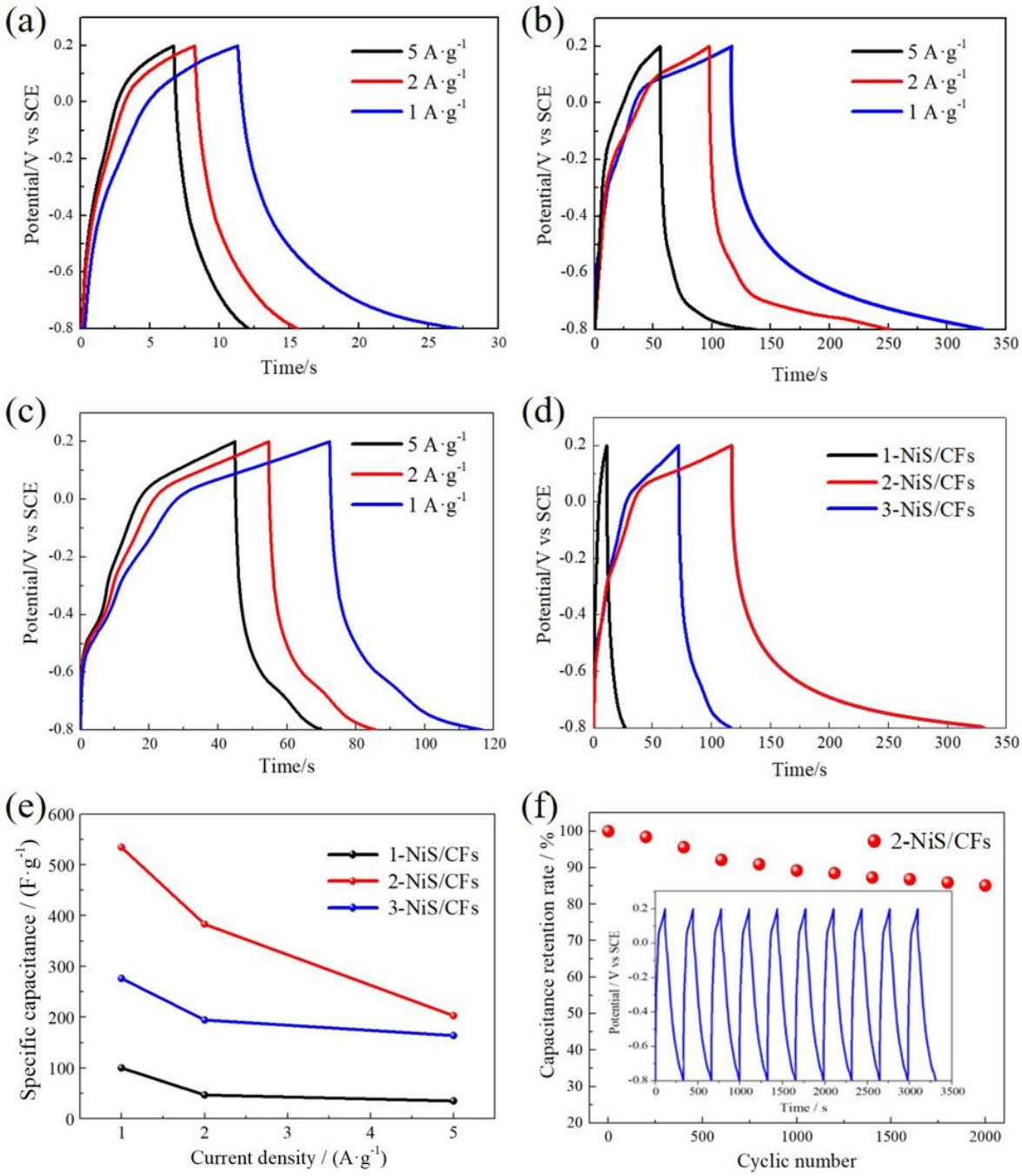

Figure 7. Galvanostatic charge-discharge curves of 1-NiS/CFs, 2-NiS/CFs and 3-NiS/CFs (**a-c**) at different current densities, and 1-NiS/CFs, 2-NiS/CFs and 3-NiS/CFs at a current density of 1 $A \cdot g^{-1}$ (**d**), the specific capacitance of the composites at different current densities (**e**), and the capacitance retention rate and cyclic performance of 2-NiS/CFs in a 3 $mol \cdot L^{-1}$ KOH solution (**f**).

As shown in Figure 8, the 2-NiS/CFs composite demonstrates an excellent energy density of 18.7 $Wh \cdot kg^{-1}$ at 252 $W \cdot kg^{-1}$. As the power density gradually exceeds 252 $W \cdot kg^{-1}$, the energy density is noted to gradually decrease. As the power density increases to 6000 $W \cdot kg^{-1}$, the energy density value is only 10.86 $Wh \cdot kg^{-1}$. However, it is still higher than the various metal sulfide composite materials, such as MCs@GNS@NiS[38], Ni_3S_2 nanorod array[39], CuS nanoplatelets [40], MoS_2 hierarchical nanospheres [41], $NiCo_2S_4$ nanotube arrays [42] and C/KCu_7S_4 [43]. Thus, the morphology of NiS nanosheet/CFs in the electrode material accelerates the charge transfer and promotes the electrochemical performance. Overall, the 2-NiS/CFs electrode material possesses a superior energy density even at the high power density values.

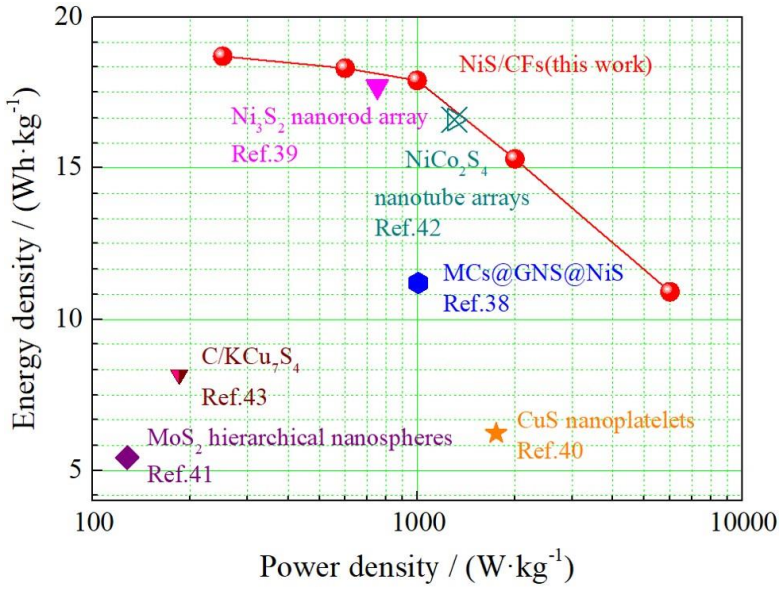

Figure 8. Ragone plots (Energy density/Power density) for the as-prepared 2-NiS/CFs.

4. CONCLUSIONS

In this study, dense and uniform NiS nanosheet was prepared on CFs to form the NiS/CFs electrode materials with controllable characteristics by using the hydrothermal method. Specifically, in the case of 2-NiS/CFs, the relatively uniform distribution of NiS is noted on the surface. The CV curve of 2-NiS/CFs exhibits the superior electric double layer and pseudo-capacitance performance. For the current density of 1 $A \cdot g^{-1}$, the electrode displays a specific capacitance of 534.8 $F \cdot g^{-1}$. After 2000 charge-discharge cycles, the capacitance retention rate of the 2-NiS/CFs composite is still appreciable at 86%. The as-developed electrode material presents an excellent cyclability as well as the optimal power (252 $W \cdot kg^{-1}$) and energy (18.7 $Wh \cdot kg^{-1}$) density values.

ACKNOWLEDGEMENTS：
We would like to express our gratitude to 2017 Open Project of the Building Energy Conservation and Science and Technology Department of Ministry of Housing and Urban-Rural Development of Beijing University of Civil Engineering and Architecture (UDC2017031812); The Science and Technology Project of Shandong Provincial Housing and Urban-Rural Department (2017-K3-002); and the Doctor Foundation of Shandong Jianzhu University (XNBS 1434).

References

1. Z.X.Tai, X.B. Yan, J.W. Lang and Q.j. Xue, *J. Power Sourses*, 199(2012) 373.
2. Y. Wang, J. Tang, B. Kong, D.S. Jia, Y.H. Wang, T.C. An, L.J. Zhang and G.F. Zheng, *RSC Adv.*, 5(2015) 6886.
3. J.D. Desai, P.K. Baviskar, K.N. Hui and H.M. Pathan, *ES Energy Environ.*, 2(2018) 21.
4. L. Zhang, M.N. Ou, H.C. Yao, Z.H. Li, D.Y. Qu, F. Liu, J.C. Wang, J.S. Wang and Z.J. Li, *Electrochim. Acta*, 186 (2015) 292.
5. Z.N. Yu, L. Tetard, L. Zhai and J. Thomas, *Energy Environ. Sci.*, 8 (2015) 702.
6. D.L. Jiang, J. Li, C.S. Xing, Z.Y. Zhang, S.C. Mengand M. Chen, *ACS Appl. Mater. Interfaces*, 7 (2015) 19234.
7. F. Beguin, V. Presser, A. Balducci and E. Frackowiak, *Adv. Mater.*, 26 (2014)2219.
8. X.F. Wang, X.H. Lu, B. Liu, D. Chen, Y.X. Tong and G.Z. Shen, *Adv. Mater.*, 26 (2014) 4763.
9. X.H. Lu, M.H. Yu, G.M. Wang and Y.X. Li, *Energy Environ. Sci.*, 7 (2014) 2160.
10. Q.H. Wang, L.F. Jiao, H.M. Du, Y.C. Si, Y.J. Wang and H.T. Yuan, *J. Mater. Chem.*, 22 (2012) 21387.
11. D.W. Wang, F. Li and H.M. Cheng, *J. Power Sources*, 185 (2008) 1563.
12. W.J. Zhou, K. Zhou, X.J. Liu, R.Z. Hu, H. Liu and S.W. Chen, *J. Mater. Chem. A*, 2(2014) 7250.
13. L.M. Dai, D.W. Chang, J.B. Back and W. Lu, *Small*, 23 (2012) 1130.
14. V.T. Le, H. Kim, A. Ghosh, J. Kim, J. Chang, Q.A. Vu, D.T. Pham, J.H. Lee, S.W. Kim and Y.H. Lee, *ACS Nano*, 7 (2013) 5940.
15. M. Huang, F. Li, J.Y. Ji, Y.X. Zhang, X.L. Zhao and X. Gao, *CrystEngComm*, 16 (2014) 2878.
16. F.I. Dar, M.R. Kevin and E.S. Mohammed, *Nanoscale Res. Lett.*, 8 (2013) 363.
17. F. Cao, G.X. Pan, X.H. Xia, P.S. Tang and H.F. Chen, *J. Power Sources*, 264 (2014) 161.
18. M. Wang, J. Yang, S.Y. Liu,C.Hu, S.F. Li and J.S. Qiu, *ACS Appl. Mater. Interfaces*, 11 (2019) 26235.
19. D.X. Guo, X.M. Song, L.C. Tan, H.Y. Ma, W.F. Sun, H.J. Pang, L.L. Zhang and X.M. Wang, *Chem. Eng. J.*, 356 (2019) 955.
20. X. Wang, S. Chen, D.H. Li, S.L. Sun, Z. Peng, S. Komarneni and D.J. Yang, *ACS Sustainable Chem. Eng.*, 6 (2017) 633.
21. S. Nandhini, A. Mary and G. Muralidharana, *Appl. Surf. Sci.*, 449 (2018) 485.
22. T.F. Yi, Y. Li, Y.M. Li, S.H. Luo and Y.G. Liu, *Solid State Ionics*, 343 (2019) 115074.
23. Y.X. Liu, Z.X. Zhou, S.P. Zhang, W.H. Luo and G.F. Zhang, *Appl. Surf. Sci.*, 442 (2018) 711.
24. J.Q. Yang, X.C. Duan, W. Guo, D. Li, H.L. Zhang and W.J. Zheng, *Nano Energy*, 5 (2014) 74.
25. A. Singh, S.K. Ojha, M. Singh and A.K. Ojha, *Electrochim. Acta*, 349 (2020) 136349.
26. W.S. Niu, Z.Y. Xiao, S.F. Wang, S.R. Zhai, L.F. Qin, Z.Y. Zhao and Q.D. An, *J. Alloys Compd.*, 853 (2020) 157123.
27. Y.G. Guo, J.S. Hu and L.J. Wan, *Adv. Mater.*, 20 (2008) 2878.
28. S.J. He, W. Chen, *Nanoscale*, 7 (2015) 6957.
29. X.Y. Cai, R.V. Hansen, L.L. Zhang, B.S. Li, C.K. Poh, S.H. Lim, L.W. Chen, J.L. Yang, L.F. Lai, J.Y. Lin and Z.X. Shen, *J. Mater. Chem. A*, 3(2015) 22043.
30. A. Wang, H.L. Wang, S.Y. Zhang, C.J. Mao, J.M. Song, H.L. Niu and B.K. Jin, *Appl. Surf. Sci.*,

282 (2013) 704.
31. J. Wu, F.X. Wei, Y.W. Sui, J.Q. Qi and X.P. Zhang, *Int. J. Hydrogen Energy*, 45 (2020) 19237.
32. J.X. Dong, S.J. Li and Y. Ding, *J. Alloys Compd.*, 845 (2020) 155701.
33. X.T. Zhang, Q.F. Lu, H. Liu, K. Li and M.Z. Wei, *Appl. Surf. Sci.*, 528 (2020) 146976.
34. P. Dhaiveegan, Y.K. Hsu, Y.H. Tsai, C.K. Hsieh and J.Y. Lin, *Surf. Coat. Technol.*, 350 (2018) 1003.
35. K. K. Upadhyay, T. Nguyen, T.M. Silva, M.J. Carmezim and M.F. Montemor, *Mater. Chem. Phys.*, 216 (2018) 413.
36. L.B. Dong, C.J. Xu, Y. Li, Z.H. Huang, F.Y. Kang, Q.H. Yangand X. Zhao, *J. Mater. Chem. A*, 4(2016) 4659.
37. D.A. Aikens, *J. Chem. Educ.*, 60 (2004) 669.
38. Y.J. Li, K. Ye, K. Cheng, J.L. Yin and G.L. Wang, *J. Power Sources*, 274 (2015) 943.
39. J. Wen, S.Z. Li, K. Zhou, Z.C. Song, B.R. Li, Z. Chen. T. Chen, Y.X. Guo and G.J. Fang, *J. Power Sources*, 324 (2016) 325.
40. C. JustinRaj, B.C. Kim, W.J. Cho, W.G. Lee, Y. Seo and K.H. Yu, *J. Alloys Compd.*, 586 (2014) 191.
41. M.S. Javed, S.G. Dai, M.J. Wang, D.L. Guo, L. Chen, X. Wang, C.G. Hu and Y. Xi, *J. Power Sources*, 285 (2015) 63.
42. H.C. Chen, J.J. Jiang, L. Zhang, D.D. Xia, Y.D. Zhao, D.Q. Guo, T. Qi and H.Z. Wan, *J. Power Sources*, 254 (2014) 249.
43. S.G. Dai, Y. Xi, C.G. Hu, X.L. Yue, L. Cheng and G. Wang, *J. Power Sources*, 263 (2014) 175.